RSC Advances

ROYAL SOCIETY OF CHEMISTRY

www.rsc.org/advances

RSC Advances

RSCPublishing

PAPER

Mechanism investigation on up and down conversion of Er^{3+} and Gd^{3+} co-doped $YTiNbO_6$ phosphors

Cite this: DOI: 10.1039/x0xx00000x

ZhichaoYu [a], Guangjun Zhou [a,*], Juan Zhou [b], Haifeng Zhou [a], Peng Kong [a], Yaqiang Wu [a], Huining Huang [a], Xiaoqiang Yu [a], Xingshuang Zhang [a] and Ruoyao Zhang [a]

Received 00th January 2012,
Accepted 00th January 2012

DOI: 10.1039/x0xx00000x

www.rsc.org/

$YTiNbO_6$ phosphors doped with Er^{3+}, Gd^{3+} were synthesized via a facile sol-gel and combustion approach. The crystal structure, particle morphology were characterized and the phonon energy was investigated in detail. The up-conversion emission excited with 980 nm and down-conversion emission excited with 378 nm of Er^{3+} with different concentrations were analysed. They both have strong green emission peaks at 522 and 552 nm but the red emission peak at 668 nm only appears in up-conversion. Furthermore, the Er^{3+} quenching concentration for up-conversion is higher than that for down-conversion because the up-conversion is a complex multiple stepwise processes which includes the energy transfer, phonon-assisted energy transfer and excited state absorption that can accept a wider range of Er^{3+} doped concentration. Moreover, the influence of co-doped Gd^{3+} on morphology and particle size was also explored. The Gd^{3+} had a great effect on up and down conversion emission intensity as well as the decay time of up-conversion by changing the structure distortion, vibration frequencies and surface-defects.

Introduction

Rear-earth doped phosphors which not only can effectively convert ultraviolet light into visible light, but also have the ability to absorb near-infrared light and emit fluorescence have attracted great attention due to their potential use for fundamental and technological applications.[1-3] The emission band of Rear-earth (RE) is sharp and narrow, and its position is weakly dependent on the surround environment or the crystal field since the unique 4f-4f transitions are shielded by the outer orbitals. Besides, the up-conversion (UC) of RE has large anti-stokes shifts up to 500 nm.[4] With those excellent and unique photoluminescent features, RE doped UC phosphors have a large number of potential applications such as biomedicine, solar cells, luminescent labels, photochemical catalysis, detector, and temperature sensor.[5-11] In the energy transfer of UC, in order to achieve multi-photon UC, the RE ions should have energy level scheme with equally spaced intermediate states. While the RE co-doping such as Yb-Er, Yb-Tm, Yb-Ho, Yb-Tb, Yb-Er-Tm have been explored in diverse host materials since Yb^{3+} can act as an sensitizer to absorb near-infrared of 980 nm efficiently and transfer to luminescence center.[12,13] Yb^{3+} sensitized materials have been well investigated in bulk and nanoscale materials.[14] Therefore, we focused our work on the less-studied single Er^{3+} doped UC phosphors where Er^{3+} not only is sensitizer but also act as luminescence centre since Er^{3+} in $4f^{11}$ configuration has an unique energy level structure to facilitate IR-to-visible multi-photon up-conversion and multi-colour emission. The phosphors doped with Er^{3+} exhibited preferential green and red emission.

Inorganic oxide compounds doped with RE ions is a class of phosphors available for many photonic applications due to their exceptional thermal and chemical stability, luminescence properties and environmental friendliness.[15] As a typical euxenite-type compound, $YTiNbO_6$ with space group Pbcn has attracted much attention attributed to its potential application as a novel host material since its information was first reported in 1974.[16, 17] What is more, our previous work has demonstrated that $RETiNbO_6$ (RE=Y、La) doped with Eu^{3+}, Er^{3+}, Dy^{3+} and Ho^{3+} have great down-conversion (DC) emission by reasons of the RE^{3+} doped into $YNbTiO_6$ host may offer more probabilities of gaining abundant multi-stage transition pathways and broad-distributing emission spectra.[18-21] However, to the best of our knowledge, there are few reports about the UC of $YTiNbO_6$. On the one hand, Y^{3+} can be easily replaced by RE^{3+}, which induced some novel up-conversion luminescence (UCL) phenomena without any change compensation problems. On the other hand, the low phonon energy as well as the crystal symmetry and microstructure of $YTiNbO_6$ are also benefit to the UCL.

In this study, Er^{3+} and Gd^{3+} co-doped $YTiNbO_6$ phosphors have been prepared through a facile sol-gel and combustion approach. The crystal structure, morphology and the concentration quenching effect on UC and DC emission were investigated. Furthermore, UC has multiple mechanisms of electronic transitions such as stepwise photo excitation, energy transfer, cross relaxation and non-radiative relaxation processes. The electronic transition and the energy transfer as well as phonon energy of $YTiNbO_6$ for UC and DC processes were systemically studied. The difference of the concentration quenching mechanism for UC and DC was contrasted. What is more, the behaviour of co-doping Gd in $YTiNbO_6$: 4% Er affected the crystallinity and the symmetry of the local field around

Er^{3+} and had a great influence on the UCL and down-conversion luminescence(DCL) intensity.

Experimental

Synthetic procedures

Pure and doped $YTiNbO_6$ phosphors were prepared by a facile sol-gel combustion process just like our previous work.[20-21] Erbium oxide (Er_2O_3), yttrium oxide (Y_2O_3), gadolinium oxide （Gd_2O_3, Niobium oxide (Nb_2O_5), tetra-n-butyl titanate ($Ti(C_4H_9O)_4$), citric acid ($C_6H_8O_7{\cdot}H_2O$) and ammonium nitrate (NH_4NO_3) were purchased form Sinopharm Chemical Reagent Beijing and used as the starting materials. Yttrium nitrate($Y(NO_3)_3$), erbium nitrate ($Er(NO_3)_3$) and gadolinium nitrate ($Gd(NO_3)_3$) solutions were obtained by dissolving Er_2O_3 Y_2O_3, and Gd_2O_3 in diluted nitric acid at a certain mole ratio. All the regents were analytical grade without any further purification.

Typically, 0.5mmol Nb_2O_5 was dissolved with excess hydrofluoric acid (HF, 40%) in a water bath at 90 ^oC, and the pH of the solution was regulated to 9.0 by adding ammonia aqueous solution. Then, the white precipitate of $Nb_2O_5{\cdot}nH_2O$ was filtered and washed with deionized water for several times to make sure that the F^{-1} ion was completely removed. Afterward, the $Nb_2O_5{\cdot}nH_2O$ was dissolved with $Ti(C_4H_9O)_4$ and citric acid with the mole ratio of 1:1:4 at 80 ^oC. Then, RE nitrate and ammonium nitrate were added into the solution. The mole ratio of citric acid and ammonium nitrate was 1:5. While citric acid used as complexant and ammonium nitrate used as fuels for the combustion process. The obtained solution was mixed homogeneously under continuous stirring at 85 ^oC until sol formed. After the water was evaporated, the transparent sol turned into yellow gel with high viscosity. The gel was dried at 110 ^oC for 24h to form the yellow xerogel. Then, the xerogels were introduced into crucibles, and directly transferred into a muffle furnace. The xerogels obtained were kept at the calcining temperature of 550 ^oC for 15min, then rose to 800, 900, 1000 and 1100 ^oC for 1 h, and then cooled down to room temperature in the furnace. Finally, all samples were ground into powder for characterization.

Characterization

The phase composition and structure were examined by X-ray powder diffraction patterns (Germany Bruker Axs D8-Avance X-ray diffractometer with graphite monochromatized Cu Kα irradiation (λ = 1.5418 Å)), and the data were collected over the 2θ range of 10^o - 70^o. The morphology and composition were characterized by scanning electron microscopy (SEM; Hitachi, S-4800) attached with the energy dispersion X-ray spectra (EDS, Horiba, EMAX, Energy, EX-350). Thermal analyses of the powder dried at 110 ^oC for 24 h was carried out from 30 to 1200 ^oC by using thermos gravimetry-differential thermal analyser (TG-DTA) (PerkinElmer Corporation, Diamond TG-DTA) with constant heating rate of 20 $^oC{\cdot}min^{-1}$. Raman spectroscopy measurements were performed on a Lab Ram Aramis (Thermo Nicolet. American. 1064 nm laser). UCL spectra were recorded using a SpectroPro300i and a power tuneable 980 nm semiconductor laser (0–800 mW). UCL decay curves were measured with a customized phosphorescence lifetime spectrometer (FSP920-C, Edinburgh) equipped with a digital oscilloscope (TDS3052B, Tektronix) and a tuneable mid-band Optical-Parametric Oscillator (OPO) pulse laser as the excitation source (410-2400 nm, 10 Hz, pulse width of 5 ns, Vibrant 355II, OPOTEK). The up-conversion of quantum yields were measured by Quanta Master-400 with a 980 nm DPSS laser. DCL spectra were recorded on a fluorescence spectrophotometer (JEOL, F-4500). All the measurements were performed at room temperature.

Results and discussion

Structure and morphology analysis

The phase purity of the as-prepared pure and doped $YNbTiO_6$ phosphors was measured by XRD. While Fig. 1 shows the different samples agree well with the euxenite-type $YTiNbO_6$ (Joint Committee on Powder Diffraction Standards JCPDS File Card No. 01-83-1318) without redundant peaks or phases. Fig. 1(a) shows with the annealing temperature rising from 800 to 1100 ^oC， the diffraction peaks successively become shaper and stronger which suggests the crystallinity becomes better and the size of sample gets bigger. Fig. 1(b) presents the pure Er^{3+} doped and Er^{3+}, Gd^{3+} co-doped samples that can well match with euxenite-type $YNbTiO_6$. It confirms that the doped ions successfully enter in the host materials and no distinct Er^{3+} or Gd^{3+} related phases such as Er_2O_3, Gd_2O_3 or Y_2O_3 appear. This can be explained that the Y^{3+} can be certainly replaced by appropriate Er^{3+} and Gd^{3+}, since they have similar physical properties and co-ordination structure.[21] Furthermore, the inset of Fig.1 (c) shows the diffraction peak (311) are slightly shifted to a higher degree when Er^{3+} or Er^{3+}, Gd^{3+} doped into the host materials since the radius of doped ions Er^{3+}(1.19 Å,CN=8) , Gd(1.14 Å,CN=8) are bigger than Y^{3+}（1.02 Å,CN=8）.[20] The larger-sized Er^{3+}, Gd^{3+} occupied smaller-sized Y^{3+} sites, leading to the lattice distortion effect and the increasing of the lattice parameters and volume accordingly.[22] From the analysis of the XRD patterns, it can be concluded that the doped ions have been successfully doped into the $YTiNbO_6$ host lattices.

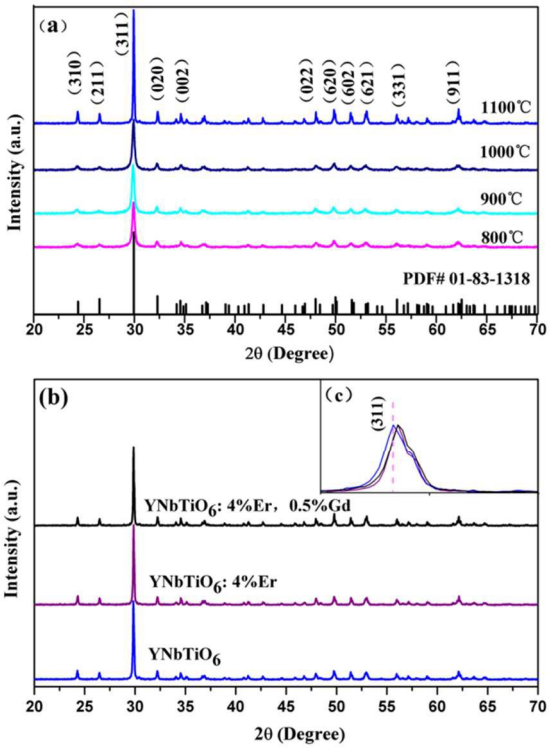

Fig. 1 (a) XRD patterns of the as-synthesized $YNbTiO_6$: 4%Er, 0.5% Gd with different temperature. (b) Pure $YNbTiO_6$, 4%Er single doped and 4% Er，0.5%Gd co-doped phosphors. (c) Comparison of the samples as-synthesized from 2 θ of 29.0 to 31.0 degree.

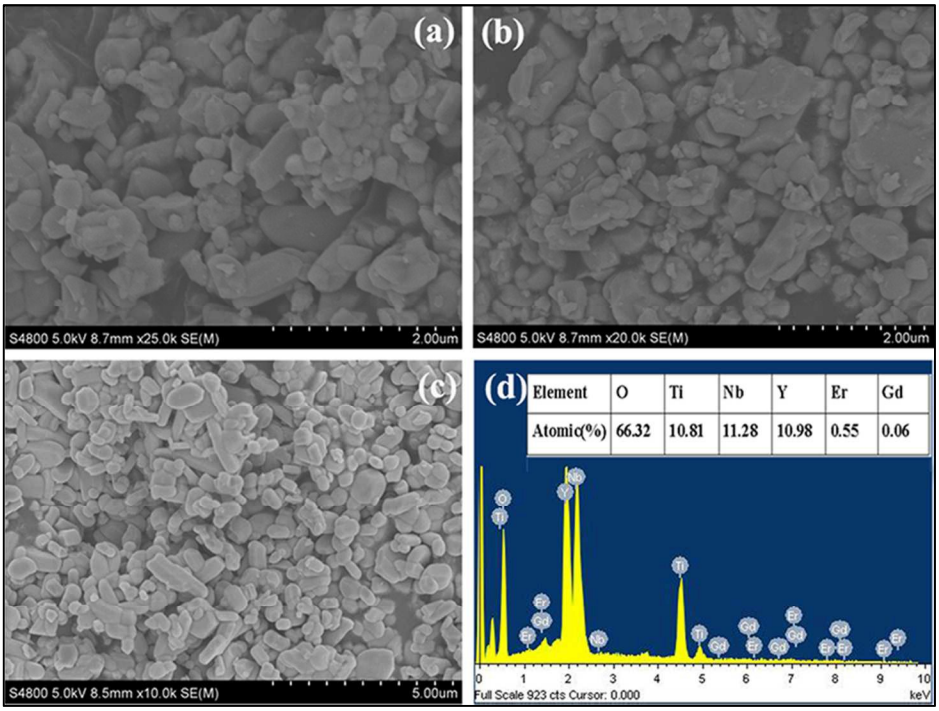

Fig. 2 SEM micrographs of the as-synthesized phosphors prepared at 1100°C: (a) $YNbTiO_6$, (b) $YNbTiO_6$:4% Er, (c) $YNbTiO_6$: 4% Er, 0.5% Gd, (d) The EDS spectrum of $YNbTiO_6$: 4% Er, 0.5% Gd sample and the inset shows the atom percent of all elements.

Typical SEM pictures of the pure and doped phosphors prepared at 1100 ^oC are presented in Fig. 2. While higher annealing temperature leads to the samples agglomeration and irregular shapes. Fig. 2(a) displays the pure $YTiNbO_6$ shaped blocks or plates with scale of 500-800 nm. The morphology of $YNbTiO_6$: 4 % Er shows in Fig. 2(b). It has similar shapes with pure $YTiNbO_6$ and its size is about 450-600 nm which is smaller than pure $YTiNbO_6$. Fig. 2(c) exhibits the image of $YNbTiO_6$: 4 % Er, 0.5 % Gd. Its morphology becomes more uniform and weaker agglomeration and the size is about 400-550 nm. The decreasing crystallite size can be attributed to an enhanced nucleation versus crystal growth upon Gd^{3+} substitution. [23] Fig. S1 shows the SEM micrographs of the as-synthesized phosphors prepared with different concentration of Gd^{3+}. Compared with the undoped Gd^{3+} sample, the morphology of samples came into nanorod. With increasing the Gd^{3+} concentrations from 0.5% to 3%, the length of nanorod became longer while the radius of the nanorod became shorter. Furthermore, the EDS spectrum of co-doped sample is presented in Fig. 2(d) where the ratio of M (Y, Er, Gd)/Ti/Nb/O is 1.04:0.97:1.01:5.97, near to 1:1:1:6, indicating that the sample is probably composed of $YNbTiO_6$. The inset shows the ratio of Y/Er/Gd is 0.947:0.047:0.005, close to 0.945:0.04:0.005,which indicates that corresponding Er^{3+} and Gd^{3+} ions were successfully combined into the host lattice.

The structure of euxenite-type $YTiNbO_6$ is shown in Fig. 3. Nb^{5+} and Ti^{4+} ions locate on the same crystallographic position. The double-layer distorted $Ti(Nb)O_6$ octahedra join together by sharing edge or corner. Each of the YO_8 polyhedra sharing edge with four others forms a single layer. Fig. 3(b), (c) show the polyhedron of $Ti(Nb)O_6$ and YO_8. While the site of cations for $YTiNbO_6$, the Y^{3+} ions occupy a $C_s^{xy}(4)$ site and the Ti/Nb ions occupy $C_1(8)$ site of general symmetry. [24] The oxygen atoms occupy three different sites of $C_1(8)$ as O_1, O_2 and O_3. O_1 and O_2 sites are tetrahedraly coordinated with two Ti(Nb) and two Y^{3+} cations , while O_3 is linked with four Ti(Nb) cations. [25]

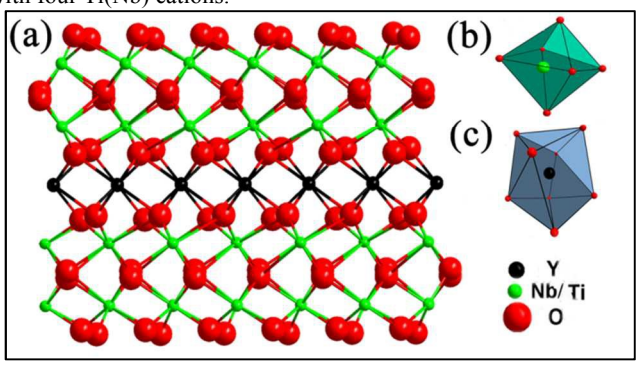

Fig. 3 (a) Three-dimensional space crystal structure of $YNbTiO_6$, (b) distorted $Ti(Nb)O_6$ octahedra, (c) YO_8 irregular polyhedron.

The TG-DTA curves of Er, Gd co-doped $YNbTiO_6$ xerogel powders dried at 110 ^oC for 24h are shown in Fig. 4. As the temperature heated to 293 ^oC, the TG cave displays the first weight loss which is about 73.64%, accompanied by the weak endothermic peaks around 161 ^oC and the exothermic peaks at 290 ^oC in the DTA cave. The weight loss is due to the evaporation of water and the combustion of organic components such as citric acid or the remaining organic components from tetra-n-butyl titanateand decomposition. The endothermic peaks are owing to the evaporation of water and the exothermic peaks are owing to the cross-link effect and the combustion of organic components. In the range of 293-563 ^oC, the second weight loss stage is because of the further combustion

of the citrate and the organic remains, accompanied by a broad exothermic peak in the range of 499-560 °C. The third stage of weight loss comes at the temperature between 563 and 1200 °C accompanied by one weak exothermic peak at 714 °C which can be ascribed to the process of the orthorhombic phase formation, crystallization and transition. When the temperature reaches to 1200 °C, the sample underwent no more transformations and there is nearly no weight loss in the TG curve, which proves that the sample has formed a relatively stable state.

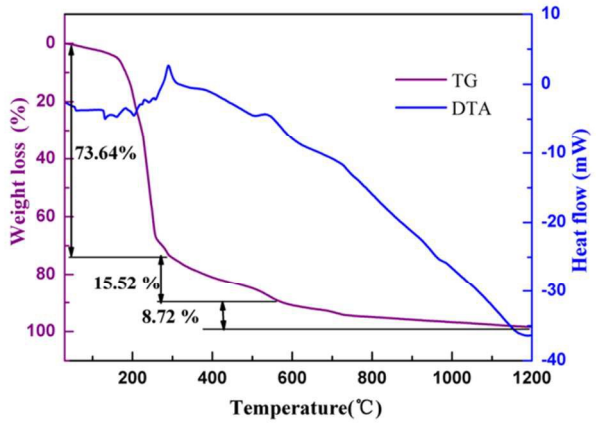

Fig. 4 TG-DTA curves of Er, Gd co-doped $YNbTiO_6$ precursor xerogel powder.

The Raman spectrum of the pure $YTiNbO_6$ is shown in Fig. 5 and main peaks are summarized in table. 1. The sample did not contains rare earth dopants in order to prevent the obscuring the Raman signal by photoluminescence. The vibration of Ti(Nb)-O bonds produce two Raman active ν_1A_{1g} and ν_2E_g modes, while the ν_1A_{1g} mode corresponds to the peak at 857.72 cm^{-1} and the ν_2E_g mode lead to the weak asymmetric shape Raman band at 630.63 cm^{-1}.[26] For wavenumber between 200 and 400 cm^{-1}, the bands are due to the symmetric bending vibrations of O-Ti(Nb)-O , corresponding to ν_3F_{1u}, ν_4F_{2g}, ν_5F_{2u} modes.[27] The last Raman band located at 155.43 cm^{-1} would be the euxenite-type lattice vibration, mainly associated with the RE ions.[24] Furthermore, the statistics confirm that the highest phonon energy of $YTiNbO_6$ is about 860 cm^{-1}, which is relative lower than some inorganic oxide compounds such as phosphate, silicate and aluminate, etc.[28] The low phonon energy is better for phonon-assisted energy transfer and may support that the $YTiNbO_6$ is a suitable host lattice for effective UCL with appropriate RE ions doping.

Table 1 Prominent Raman peaks and characteristic modes of $YTiNbO_6$

Wavenumber(cm^{-1})	Stretching vibration	Assignments
857.72	Ti-O, Nb-O	ν_1A_{1g}
636.63	Y-O, T-O, Nb-O	ν_2E_g
399.28	O-Ti-O, O-Nb-O	ν_3F_{1u}
350.51	O-Ti-O, O-Nb-O	ν_5F_{2g}
278.98	O-Ti-O, O-Nb-O	ν_6F_{2u}
226.96	O-Ti-O, O-Nb-O	ν_6F_{2u}
155.43	Lattice vibration	Lattice modes

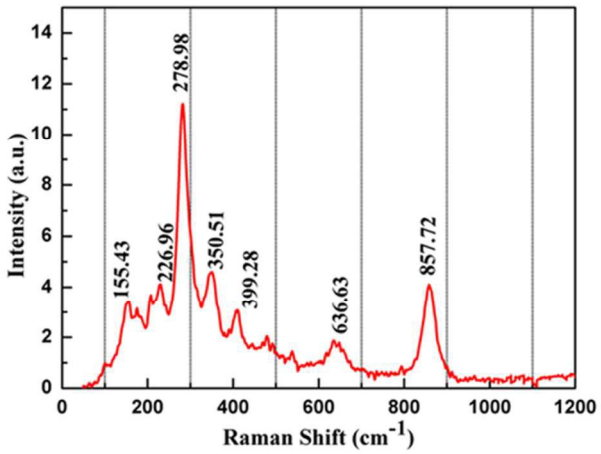

Fig. 5 Raman spectrum of pure $YTiNbO_6$ phosphor.

UC and DC emission properties

It is well known that the doping concentration and co-doped ions have a great impact on UC and DC luminescent properties. In order to reveal the concentration dependency by UCL and DCL in $YTiNbO_6$, the emission spectra with different Er^{3+} doping are shown in Fig. 6(a) and (b). Fig. 6(a) shows the DCL excited with 378 nm appears two main emission peaks centred at 522 and 552 nm and Fig. 6(b) displays the UCL excited with 980 nm that has three main emission peaks located at 522, 552 and 668 nm. All the emission peaks can be explicated by the energy transition of Er^{3+} as displayed in Fig. 6(d). The green emissions at 522 and 552 nm are due to the $^2H_{11/2} \rightarrow {}^4I_{15/2}$ and $^4S_{3/2} \rightarrow {}^4I_{15/2}$ transition .While for the red emission at 668 nm, the ground state electrons were excited to the excited state $^4F_{7/2}$ through the ETU and ESA processes and then transfered to $^4F_{9/2}$ state by multi-phonon relaxation. Whereafter the excited electrons jumped to the ground state with the transition of $^4F_{9/2} \rightarrow {}^4I_{15/2}$. Compared with the DCL, the UCL has strong red emission which can be clarified that under 980 nm excitation, the lower lever $^4F_{9/2}$ can be more effectually populated than under 378 nm excitation.[29] Furthermore, the highest intensity of UCL is achieved when doped with 4 % Er^{3+}, while for DCL, the best concentration is 2 % Er^{3+}.

To study the difference influence of Er^{3+} doping concentration on UCL and DCL, the green emission at 522 nm for UC and DC are calculated from the emission spectrum in Fig. 6(a) and (b) as shown in Fig. 6(c). It can be seen that with 378 nm excitation, the intensity rapidly rises as the doping concentration increase from 0.5% to 2% and then slowly decreases as doping concentration varies from 2% to 5%. While under 980 nm excitation, the intensity gradually goes up with the concentration increasing from 0.5% to 4% and followed with decreasing as doping concentration increase form 4% to 5%. They both increase at first and reach their own maximum values, and then decrease with raising Er^{3+} concentration. The influence of Er^{3+}concentration on UCL and DCL are different mainly from different excitation routes and quenching mechanisms.[22]

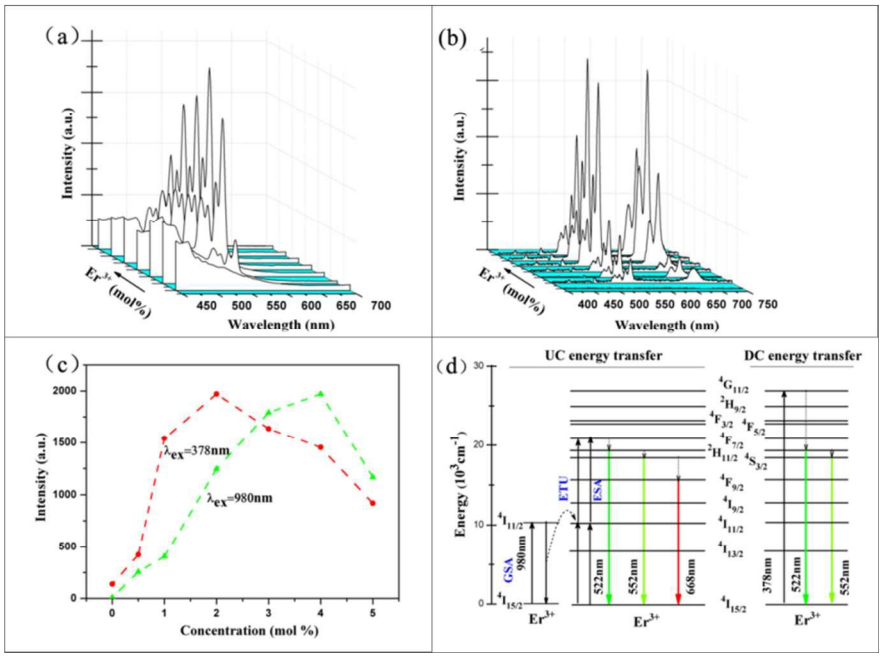

Fig. 6 (a) DC emission spectra under 378 nm excitation with doping x % mol Er^{3+}(x= 0, 0.5, 1, 2, 3, 4, 5). (b) UC emission spectra under 980 nm excitation with different concentration of Er^{3+}. (c) The intension changing of DC and UC emission spectra at 522 nm with the increase of Er^{3+} concentration. (d) Simplified energy level diagram and the UC and DC energy transfer mechanisms in Er^{3+} doped $YTiNbO_6$. Ground state absorption (GSA), excited state absorption (ESA), energy transfer up-conversion (ETU).

The luminescence intensity is mainly affected by the electron transition, non-radiative relaxation and energy transfer processes for UCL and DCL. For the DCL excited at 378 nm in Fig. 6(c), when the Er^{3+}concentration is lower than 2%,the luminescence intensity is nearly linearly proportional to the Er^{3+} concentration. This is due to that the $^2H_{11/2}$ level is populated via cascade multiphonon nonradiaive transition from $^4G_{11/2}$ while the cross relaxation（CR） between Er^{3+} ions can be disregarded. With the concentration of Er^{3+} surpassing 2%, the intensity begins to decline because the CR interactions between Er^{3+} ions begin to take effect and the concentration quenching appears. The influence of CR factor is inversely proportional to R^Q (R is the average distance between Er^{3+}ions, Q is interaction between electric-dipoles and magnetic dipoles).[29] While, the R^Q will rapidly decline with the increasing of Er^{3+} concentration， and the CR effect will be enhanced. The CR in the energy level can be describe as $^2H_{11/2} + {}^4I_{15/2} \rightarrow {}^4I_{13/2} + {}^4I_{9/2}$ (CR1) , $^2H_{11/2} + {}^4I_{13/2} \rightarrow {}^4I_{11/2} + {}^4F_{9/2}$ (CR2) and $^4S_{3/2} + {}^4I_{15/2} \rightarrow {}^4I_{9/2} + {}^4I_{13/2}$ (CR3). [30] Therefore, those CR processes reduce carrier number in $^2H_{11/2}$ and $^4S_{3/2}$ levels and lead to the fluorescence quenching in the DCL.

For the 522 nm emission band excited with 980 nm laser ,when the Er^{3+}concentration is lower than 4%, the luminescence intensity slowly increases which is different from DCL. Furthermore, the quenching concentration of Er^{3+} in UC is higher than DC and the UCL keeps increase while the DCL has reach its quenching concentration. This can be explained from the UC energy transfer in Fig. 6(d). When the Er^{3+} concentration is lower, the $^2H_{11/2}$ level is mainly populated by the excited state absorption (ESA) process. With the concentration increasing, the energy transfer between Er^{3+} will be developed. The energy transfer up-conversion (ETU) due to the strong multipolar ion-ion interactions is induced by the short distance between Er^{3+} ions. The phonon-assisted energy transfer also promotes the Er^{3+} ions at $^4I_{11/2}$ level consecutively transfers to the $^4F_{7/2}$ via the energy transfer from Er^{3+}ions at the excited $^4I_{11/2}$ level transfer to the ground level $^4I_{15/2}$. [31] The ETU process between Er^{3+} can be described as $^4I_{11/2} + {}^4I_{11/2} \rightarrow {}^4F_{7/2} + {}^4I_{15/2}$. Therefore, the ETU provides a wide range of Er^{3+}concentration and the UCL gets a higher fluorescence quenching concentration than the DCL. With the concentration of Er^{3+} surpassing4%, the intensity begins to rapidly decline which due to the energy migration and the concentration quenching appears.[32] Furthermore, the UCL excited with 785 nm laser was shown in Fig.S2 which revealed only week green emission at 522 nm and 552 nm and without red emission. This was owing to that the Er^{3+} had a little absorb at 785nm and after multi-phonon relaxation there were hardly any electrons on the excited state of $^4F_{9/2}$.

Trivalent gadolinium ions (Gd^{3+}) have a $4f^7$ electronic configuration and have many excellent characteristics when co-doped in host materials. [33, 34] Fig. 7(a) and (b) shows the DCL and UCL curves for $YTiNbO_6$:4%Er, x% Gd (x=0, 0.5, 1, 2, 3) and the inset (1), (2) are the sample of UC pictures. It is observed that incorporation of Gd ions in $YTiNbO_6$: 4% Er does not have any effect on the position of the emission band but does change the UCL and DCL intensity. While for the DCL shows in Fig. 7 (a), it is found that the emission intensity of Er^{3+} prominently increases with Gd^{3+} concentration increases to 1 % for $YTiNbO_6$: 4% Er and then decreases. The co-doped of Gd^{3+} induces higher local distortion in $YTiNbO_6$: 4% Er host lattice and increase odd-rank crystal field components which can significantly enhance the DCL intensity.[35] When the concentration of Gd^{3+} exceeds 1%, the intensity slowly decline, which may be due to the surface defects and the concentration quenching effect. Fig.S3 shown the excitation spectra of $YNbTiO_6$: 4%Er doped with different concentration of Gd^{3+} ions at the emission band at 552 nm. There were no other excitation peaks appeared except the Er^{3+} ions. The relative intensity of the excitation spectra were consistent with the DCL shown in Fig.7(a) . For the UCL shows in Fig. 7 (b), the $YTiNbO_6$: 4% Er co-doped with 0.5% Gd results a higher UC emission intensity than without Gd^{3+} doping, which can be ascribed to the fact that after Gd^{3+} modified the shape and morphology, the particles were formed

uniform nanorod which influences the structure cell distortion, bond vibration frequencies and surface defects and the changing of surrounding environment of Er^{3+} can impact energy transfer and phonon relaxation. With further increasing the concentration of Gd^{3+}, the UCL decreases evidently. This is mainly owing to that the morphology of the nanorod largely increased the surface quenching sites and the excess Gd^{3+} ions makes a significant increase of lattice distortion, defect concentration.[36]

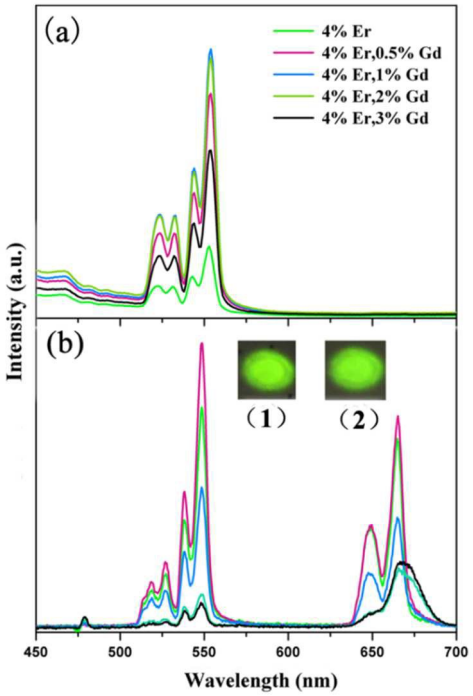

Fig. 7(a) DC emission spectra of $YTiNbO_6$: 4% Er, x% Gd(x=0.5, 1, 2, 3,), (b) UC emission spectra of $YTiNbO_6$ 4% Er, with the corresponding concentration of Gd. The inset (1) and (2) show the pictures of $YTiNbO_6$: 4% Er and $YTiNbO_6$:4%Er, 0.5%Gd excited with 980 nm laser (600 mw).

While for the UC mechanisms of $YTiNbO_6$:4% Er, 0.5% Gd, the integer n in the equation $I_{up} \propto P^n$ is the number of NIR photons absorbed to generate a higher frequency photon.[37,38] The pump power dependency is shown in Fig. 8(a). For the slope of $In(I_{up})$ versus In(P) for 552 nm and 668 nm emission bands are found to be 2.24 and 1.76 respectively which illustrates that the transition of $^4S_{3/2} \rightarrow {}^4I_{5/2}$ and $^4F_{9/2} \rightarrow {}^4I_{15/2}$ involve a two-photon absorption process. Whereas the slopes are deviated from 2, which might be caused by the multiphonon relaxation to a lower-lying state, nonradiative transition or the radiative decay to the ground state.[37] The quantum yield of $YTiNbO_6$:4% Er, 0.5% Gd was $3.03E^{-7}$ which was lower than the Er^{3+}, Yb^{3+} co-doped fluorochemical[39]. This was due to that the phonon energy of $YTiNbO_6$ was higher than the fluorochemical and Er^{3+} was acted as both sensitizer and activator sensitizer while Yb^{3+} was not adoped. Compared with fluorochemical, $YTiNbO_6$ was more stable on chemical and thermal and could be expanded the up-conversion properties in other applications fields.

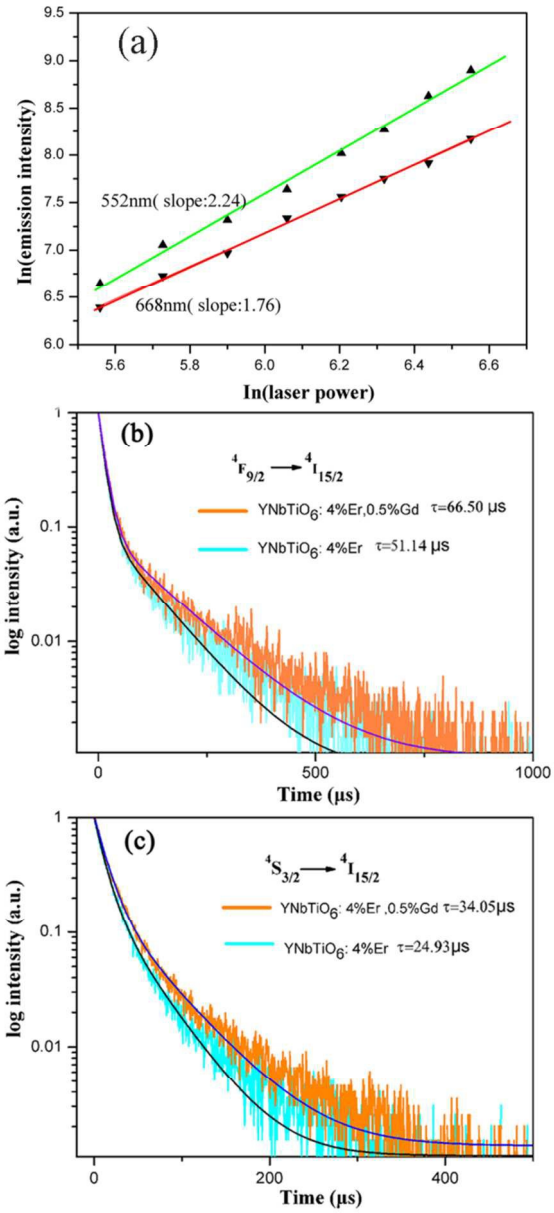

Fig. 8(a) Pump power dependence of the green and red UCL integrated intensities of $YNbTiO_6$: 4% Er, 0.5% Gd under 980 nm excitation. (b) UCL decay curves of Er^{3+} measured at 668 nm for $YNbTiO_6$: 4% Er and $YNbTiO_6$:4% Er,0.5% Gd.(c) UCL decay curves of Er^{3+} measured at 552 nm for $YNbTiO_6$:4% Er and $YNbTiO_6$: 4% Er, 0.5% Gd.

In order to full understand the influence of Gd^{3+} on the UCL of $YNbTiO_6$: 4% Er, it is necessary to compare the decay curves before and after doping Gd^{3+} ions. To quantify the decay constant, all the decay curves I(τ) are fitted with a double exponential equation:

$$I(\tau) = a_1 \exp^{(-\frac{\tau}{\tau_1})} + a_2 exp^{(-\frac{\tau}{\tau_2})} \qquad (1)$$

Where I(τ) is the luminescence intensity at the maximum of emission band, a_1 and a_2 are the exponential pre-factors and τ_1 and τ_2 are the fitted decay times. The shorter time τ_1 may be related to the surface Er^{3+} of the phosphors, while the long decay time τ_2 could be

attributed to the Er^{3+} located in the bulk phase of the phosphors. [40] Furthermore, the average decay time constant τ can be determined by the equation:

$$\tau = \frac{a_1 \tau_1^2 + a_2 \tau_2^2}{a_1 \tau_1 + a_2 \tau_2} \qquad (2)$$

Fig. 8(b) and(c) show the record decay curves of the $^4F_{9/2}$ and $^4S_{3/2}$ states of the $YNbTiO_6$: 4% Er before and after doping with 0.5% Gd. Both of the decay time increase after doping with 0.5% Gd compared with the undoped sample, which could be ascribed to the doping Gd^{3+} ions which lead to a lower symmetry of the surround environment of Er^{3+} and had an effect on the energy transfer of the UC process. What is more , the red emission decay time is found to be longer than the green emission ,which is related to that the red decay rate is lower than the green decay rate. [41]

Conclusions

Euxenite-type $YTiNbO_6$ doped with Er^{3+}, Gd^{3+} has remarkable UCL and DCL property. Single Er^{3+} doped $YTiNbO_6$, the mechanisms of UC and DC excited at 980 nm and 378 nm were characterized. Both UCL and DCL were observed strong green emission at 522 and 552 nm while the UCL also had strong red emission at 668 nm. The concentration of Er^{3+} had different effect on UCL and DCL and they had different quenching concentration of Er^{3+} due to the different depopulation routes and energy transfer. When Gd^{3+}ions co-doped in $YTiNbO_6$: 4% Er, the morphology became uniform nanorod, particle agglomeration got weaker and the particle size turned smaller. In addition, it has been found that the co-doped Gd^{3+} do not change the UC and DC emission peak position but increase their intensity through changing the surrounding environment of Er^{3+} ions, enhancing the phonon-assisted energy transfer and enhancing the symmetry breaking.

Acknowledgements

This work was supported by projects from the Chinese PLA Medical Science and Technique Foundation (CWS11J243) and the Scientific Research Foundation for the Returned Overseas Chinese Scholars, State Education Ministry.

Notes and references

[a] State Key Laboratory of Crystal Materials, Shandong University, Jinan 250100, P. R. China.

[b] Center for Disease Prevention and Control of Jinan Military Command, Jinan 250014, P. R. China.

* Corresponding author. Fax: +86 531 88361206

E-mail address: gjzhou@sdu.edu.cn

1. Y. Mao, T. Tran, X. Guo, J. Y. Huang, C. K. Shih, K. L. Wang and J. P. Chang, *Adv. Funct. Mater.,* 2009, **19**, 748.
2. G. Liu, *Chem.Soc.Rev.*, 2015, **44**, 1635.
3. N. C. Dyck, F. C. J. M. van Veggel and G. P. Demopoulos, *ACS Appl. Mater.* Inter., 2013, **5**, 11661.
4. Y. Wang, W. Xu, S. Cui, S. Xu, Z. Yin, H. Song, P. Zhou, X. Liu, L. Xu and H. Cui, *Nanoscale.*, 2015, **7** , 1363.
5. J. Han, C. Zhang, F. Liu, B. Liu, M. Han, W. Zou, L. Yang and Z. Zhang, *Analyst.*, 2014, **139**, 3032.
6. A. Sedlmeier and H. H. Gorris, *Chem. Soc .Rev.*, 2015, **44**, 1526.
7. J. Zhao, Y. Zhu, J. Wu and F. Chen, *J. Colloid. Interf. Sci*., 2015, **440**, 39.
8. F. Xin, S. Zhao, G. Jia, L. Huang, D. Deng, H. Wang and S. Xu, *Mater. Chem. Phys.*, 2012, **137**, 177.
9. X. Huang, S. Han, W. Huang and X. Liu, *Chem. Soc. Rev.*, 2013, **42**, 173.
10. R. Dey and V Kumar Rai, *Dalton Trans.*, 2014, **43**, 111.
11. C. S. Lim, *Infrared Phys. Technol.*, 2014, **67**, 371.
12. R. Krishnan and J. Thirumalai, *New J. Chem.*, 2014, **38**, 3480.
13. O. Ehlert, R. Thomann, M. Darbandi and T. Nann, *ACS Nano.*, 2008, **2**, 120.
14. W. Feng, C. Han and F. Li, *Adv. Mater.*, 2013, **25**, 5287.
15. A. K. Singh, S. K. Singh and S. B. Rai, *RSC Adv.*, 2014, **4**, 27039.
16. X. Qi, R. Illingworth, H. G. Gallagher, T. P. J. Han and B. Henderson, *J. Cryst. Growth*, 1996, **160**, 111.
17. Y. Shi, Y. Wang and Z. Yang, *J. Alloys Compd.*, 2011, **509**, 3128.
18. Q. Ma, M. Lu, P. Yang, A. Zhang and Y. Cao, *Mater. Res. Bull.*, 2013, **48**, 3677.
19. Q. Ma, M. Lu, P.Yang, A. Zhang and Y. Cao, *Luminescence*, 2014, **29**, 386.
20. Q. Ma, Y. Zhou, A. Zhang, M. Lu, G. Zhou and C. Li, *Solid State Sci.*, 2009, **11**, 1124.
21. X. Zhang, G. Zhou, J. Zhou, H. Zhou, P. Kong, Z. Yu and J. Zhan, *RSC Adv.*, 2014, **4**, 13680.
22. Y. Wang, W. Xu, S. Cui, S. Xu, Z. Yin, H. Song, P. Zhou, X. Liu, L. Xuand and H. Cui, *Nanoscale*, 2015, **7**, 1363.
23. X. Wu, J.G. Li, Q. Zhu, J. Li, R. Ma, T. Sasaki, X. Li, X. Sun and Y. Sakka, *Dalton Trans.*, 2012, **41**, 1854.
24. C.W.A. Paschoala, R.L. Moreira, C. Fantini, M. A. Pimenta, K. P. Surendranb and M. T. Sebastian, *J. Eur. Ceram. Soc.*, 2003, **23**, 2661.
25. B. P. Singh, A. K. Parchur, R. K. Singh, A. A. Ansari, P. Singh and S. B. Rai, *Phys. Chem. Chem. Phys.*, 2013, **15**, 3480.
26. S. Joseph, M. K. Suresh, J. K. Thomas, A. John and S. Solomon, *Int. J. Appl. Ceram. Technol.*, 2010, **7**, 129.
27. S. Solomon, D.B. Dhwaja, G. R. Remya, A. John and J.K. Thomas, *J. Alloys Compd.*, 2010, **504**, 151.
28. B. R. Diamente, M. Raudsepp, and F. C. J. M. Veggel, *Adv. Funct. Mater.,* 2007, **17**, 363.
29. J. Li, J. Sun, J. Liu, X. Li, J. Zhang, Y. Tian, S. Fu, L. Chen, H. Zhong, H. Xia and B. Chen, *Mater. Res. Bull.*, 2013，**48**, 2159.
30. H. Lu, W. P. Gillin and I. Hernández, *Phys. Chem. Chem. Phys.*, 2014, **16**, 20957.
31. G. Chen, T. Y. Ohulchanskyy, A. Kachynski, H. Ågren and P. N. Prasad, *ACS Nano*., 2011, **5**, 4981.
32. E. M. Chan, G. Han, J. D. Goldberg, D. J. Gargas, A. D. Ostrowski, P. J. Schuck, B. E. Cohen and D. J. Milliron, *Nano Lett.*, 2012, **12**, 3839.
33. J. Wang, Y. Cheng, Y. Huang, P. Cai, S. I. Kim and H. J. Seo, *J. Mater. Chem. C.*, 2014, **2**, 5559.
34. R. Krishnan and J. Thirumalai, *New J. Chem.*, 2014, **38**, 3480.
35. B. P. Singh, A. K. Parchur, R. S. Ningthoujam, A. A. Ansari, P. Singh and S. B. Rai, *Dalton Trans.*, 2014, **43**, 4779.
36. S. Zeng, J. Xiao, Q. Yang and J. Hao, *J. Mater. Chem.*, 2012, **22**, 9870.
37. J. Zhao, Y. Sun, X. Kong, L. Tian, Y. Wang, L. Tu, J. Zhao and H Zhang, *J. Phys. Chem. B.*, 2008, **112**, 15666.
38. F. Vetrone, V. Mahalingam and J. A. Capobianco, *Chem. Mater.,* 2009, **21**, 1847.
39. X. Li, R. Wang, F. Zhang and D. Zhao, Nano Lett., 2014, **14**, 3634
40. D. T. Klier and M. U. Kumke, *J. Phys. Chem. C.*, 2015, **119**, 3363.
41. J. Zhao, Z. Lu, Y. Yin, C. McRae, J. A. Piper, J. M. Dawes, D. Jin and E. M. Goldys, Nanoscale, 2013, **5**, 944.

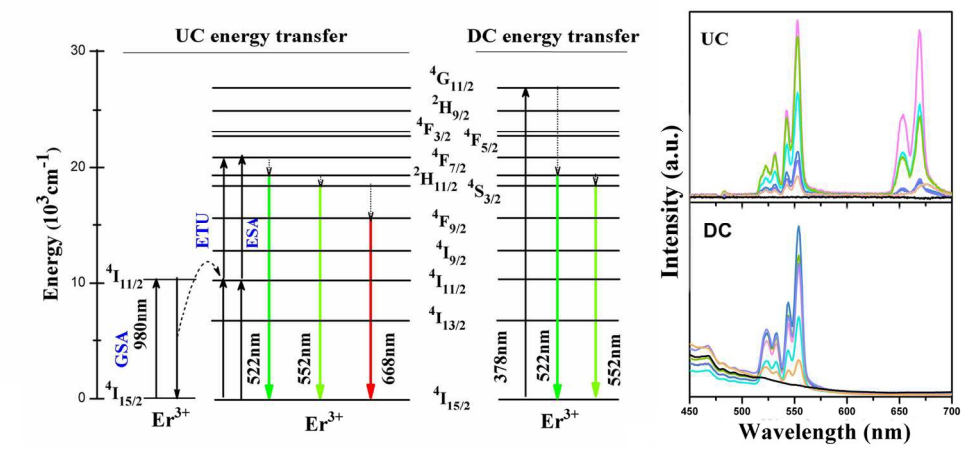

The present work focuses on the up and down conversion of YNbTiO6 with different quenching concentrations of Er3+ and Gd3+ as well as the energy transfer processes.
169x93mm (300 x 300 DPI)